JOURNAL OF
Optical Communications
and Networking

TRA: an efficient dynamic resource assignment algorithm for MCF-based SS-FONs

SHRINIVAS PETALE,[1,*] JUZI ZHAO,[2] AND SURESH SUBRAMANIAM[1]

[1]Department of Electrical and Computer Engineering, The George Washington University, Washington DC, 20052, USA
[2]Department of Electrical Engineering, San Jose State University, San Jose, California, 95192, USA
*Corresponding author: srpetale@gwu.edu

Received 2 February 2022; revised 27 April 2022; accepted 28 April 2022; published 20 May 2022

Service provisioning can be enhanced with spectrally spatially flexible optical networks (SS-FONs) with multicore fibers; however, intercore crosstalk (XT) is a dominant impairment that complicates the problem of maintaining the quality of transmission (QoT) and resource allocation. The selection of modulation formats (MFs), due to their unique XT sensitivities, further increases the complexity. The routing, modulation, core, and spectrum assignment (RMCSA) problem must select the resources carefully to exploit the available capacity while meeting the desired QoT. In this paper, we propose an RMCSA algorithm called the tridental resource assignment (TRA) algorithm for transparent SS-FONs, and its variant, translucency-aware TRA (TaTRA), for translucent SS-FONs. TRA balances three different factors that affect network performance under dynamic resource allocation. We consider translucent networks with flexible regeneration and with and without modulation and spectrum conversion. Our resource assignment approach includes both an offline network planning component to calculate path priorities and an online/dynamic provisioning component to allocate resources. Extensive simulation experiments performed in realistic network scenarios indicate that TRA and TaTRA significantly reduce the bandwidth blocking probability by several orders of magnitude in some cases.

https://doi.org/10.1364/JOCN.455426

1. INTRODUCTION

The recent increase in Internet usage for online gaming, video streaming, cloud services, and 5G and 6G communications has put pressure on the backbone optical network and has led to imminent capacity exhaustion. Elastic optical networks (EONs) divide and break down the flexible spectrum into small frequency slices (FSs), which can be concatenated to fulfill the requested capacity of lightpath requests if spectrum continuity is maintained [1]. Spatial division multiplexing (SDM), which can be implemented using multicore, multimode, or multiparallel fibers, is another viable solution to scale fiber capacity. We consider spectrally spatially flexible optical networks (SS-FONs) employing multicore fibers (MCFs) in this paper that enable parallel transmission of optical signals in multiple fiber cores. SS-FONs allow flexible spectrum choices on multiple spatial dimensions in the same fiber and are expected to be the future of optical transport networks [2]. In MCF-based SS-FONs, lightpaths are routed through cores on the links on the route with a set of contiguous and continuous FSs. SS-FONs with MCFs can offer the desired resources to mitigate the capacity crunch. However, the parallel transmission of signals through MCFs degrades the quality of transmission (QoT) because of intercore crosstalk (XT) between coupled cores, which makes the reception of signals difficult [2,3]. The routing, modulation, core, and spectrum assignment (RMCSA) problem in SS-FONs is a very challenging problem, and it is necessary to design efficient RMCSA algorithms to assign the available resources to dynamically arriving lightpath requests while maintaining the desired QoT levels.

Service provisioning can be eased with translucent networks. In translucent networks, 3R regenerators located at intermediate nodes of a lightpath that perform retiming, reshaping, and reamplification of optical signals improve the QoT. Regenerators enable the use of higher modulation formats (MFs) by mitigating the effect of limited transmission reach (TR), defined as the maximum distance a signal can be transmitted without regeneration. The change in the network dynamics in the presence of regenerators poses an additional challenge for RMCSA [4]. Proper spectrum selection ensures that the XT levels in the network are low and resources are available for future connections. Multipath routing [with shortest paths (SPs) preferred] is another suggested approach to reduce the accumulation of XT [5]; however, it poses the problem of uneven load distribution, which creates a scarcity of resources for future connections. Spectrum assignment becomes even more challenging with the selection of multi-XT-sensitive MFs. Higher MFs are more spectrum-efficient and therefore require less spectrum to satisfy a demand; on the other hand, they are more sensitive to XT. Higher sensitivity

to XT results in smaller TRs. In an MCF link, due to weakly coupled cores, when a highly sensitive MF is selected on a particular core for a lightpath, it blocks the overlapping spectrum (OS) on adjacent cores (OsaC) from being occupied as long as this lightpath remains in the network so that the QoT requirement can be met. Selecting a core with more adjacent cores leads to blocking of more spectrum in the case of highly sensitive MFs. Thus, each spectrum choice causes different amounts of XT due to ongoing connections on the OS. On the other hand, higher MFs require less spectrum for the same lightpath bit rate. A well-designed algorithm that handles the tradeoff between spectrum usage and XT levels with the selection of MF, core, and spectrum is therefore needed.

In this paper, we propose an efficient RMCSA algorithm called a tridental resource assignment (TRA) algorithm for transparent networks (TpNs) and translucency-aware TRA (TaTRA) for translucent networks. The word *tridental* refers to the fact that the algorithm considers three factors of spectrum assignment that affect performance: the available (XT-limited) capacity in the network, the spectrum requirement, and the spectrum fragmentation. TRA includes both an offline component and an online/dynamic component. The offline component is to balance the load distribution in the network and involves the use of mixed integer linear programming (MILP) to obtain path priorities for a lightpath's route. The online component selects the route, core, MF, and spectrum for the arriving lightpath in an efficient manner. This paper makes the following three contributions: (a) Two RMCSA algorithms–TRA and TaTRA—are designed, respectively, for TpNs and translucent networks. These algorithms are different from prior algorithms in that they explicitly consider the network's capacity to accommodate future connections in the resource assignment process. (b) Extensive numerical results demonstrate the superior performance of TRA and TaTRA over other algorithms. (c) A detailed analysis of the bandwidth blocking probability (BBP) in terms of the utilization of MFs and SPs and types of blocking is conducted.

An early version of the TRA algorithm was first proposed in our recent work in [6]. This paper extends and improves upon that work in several ways. First, we propose an enhanced version of TRA that chooses MFs even more efficiently. Second, we extend the algorithm to translucent networks and develop TaTRA. Third, we present an approach to compute the path priorities for translucent networks. Fourth, we investigate the effect of relaxing the core continuity constraint and of the effects of modulation conversion (MC) and spectrum conversion (SC) offered by regenerators. Finally, we present a more extensive set of numerical results to demonstrate the effectiveness of TRA and TaTRA over other algorithms.

This paper has seven additional sections. A brief survey of related work is presented in Section 2. The network model and problem statement are introduced in Section 3. The path priority computation using MILP is presented in Section 4. Formal definitions and an example to understand the calculations are presented in Section 5. The TRA and TaTRA algorithms are introduced in Section 6. Section 7 presents simulation results, and Section 8 concludes the work.

2. RELATED WORK

Recently, there has been an emphasis on the development of algorithms and technologies to exploit SDM functionalities [2,7]. In [8], the routing, spectrum, and core assignment (RSCA) problem is studied for an MCF-based SDM EON and the performance is improved with the consideration of the core priority [9] and spectrum partitioning [10]. The sequence of searching for core, mode, and spectrum for assignment affects the network performance [10]. A joint approach to reduce XT and fragmentation for on-demand assignment of core and spectrum is studied in [11]. The approach to account for XT is selected based on the trade-off between computational time and accuracy in the utilization of resource assignment. These approaches are worst-case XT estimation [12–14], best-case XT avoidance [10,11], and exact evaluation [10,15]. Enhanced searching criteria are also proposed to improve the first-fit algorithm. A core selection-based enhanced first-fit algorithm is proposed in [16]. A priority-based enhanced XT-avoidance approach is presented in [17] for multimode MCFs. An XT-aware first-fit approach with exhaustive search of the lower index of spectrum over K SPs is studied in [13].

In [15], three approaches are proposed to solve the RSCA problem in SDM-EON: node-arc-based integer linear programming (ILP) and its faster variant MILP, in addition to an XT-aware heuristic algorithm. In [18], Yang *et al.* address the routing, modulation, spectrum and transceiver assignment (RMSTA) problem in an EON and study the effect of transceiver placement on network performance. An ILP solution with tuned weighting coefficients to balance the spectrum and transceiver usage is proposed. A virtual-network-based heuristic algorithm to reduce computation complexity while reducing the resource consumption is proposed. In [19,20], Klinkowski and Walkowiak study the improvement in performance with signal regeneration and MC. They consider static traffic, unlike the studies in [18,21], and use the known traffic and its pattern to increase the transceiver and spectrum utilization in long-haul networks. Back-to-back (B2B) regeneration is used to adaptively choose the path and regeneration points to optimize the transponder placement and spectrum utilization in [21]. The worst case XT estimation in SS-FONs is studied in [22] and the effect of XT when B2B regeneration is allowed is studied in [23]. The transponder placement problem with B2B regeneration in the presence of XT is studied in [24]. Similarly, a data analytics approach along with B2B, in which the algorithm uses network information and a dynamic routing algorithm to gain extra knowledge, is proposed for transponder placement decisions in [25]. A route, modulation, core, mode, and spectrum allocation scheme for few-mode MCFs with fractional joint switching is proposed in [26,27]. The better performing conservative resource allocation scheme offers lower blocking and better QoT, but with a higher computation time and a higher number of required lasers. XT-aware and fragmentation-aware algorithms, with the use of a splitting technique, are proposed to improve spectrum utilization in [28]. An RMCSA algorithm based on programmable nodes and static reconfigurable optical add-drop multiplexers (ROADMs) is proposed in [29]. The enhanced and flexible switching architecture is used for better spectrum utilization.

In [30], Agrawal *et al.* propose a proactive approach to mitigate the effect of XT by sorting route-core pairs on the basis of spectrum utilization. The sorting helps avoid the XT-sensitive resource choices. Similarly, static planning before dynamic provisioning is studied in [31] to tackle the issue of the variation in security levels due to a change in XT levels. A weighted ILP and a heuristic are designed to increase spectrum utilization and reduce average intercore XT. The network is treated as a graph with secure nodes and links, and normal provisioning is done only when the trust-level thresholds are met.

In this paper, we combine offline planning and dynamic network provisioning to balance the trade-off between spectrum utilization and the XT levels in the network. We will show that our algorithm outperforms several algorithms from the literature. Regenerators in translucent networks allow the use of higher MFs (i.e., increased spectral efficiency) compared to TpNs, which in turn improve spectrum utilization and change the pattern of XT accumulation in the network. In this paper, we propose TRA, a network capacity-aware RMCSA algorithm for a TpN and TaTRA for two scenarios of a translucent network with the aim to balance the trade-off and lower the BBP with a strategic selection of resources.

3. NETWORK MODEL AND PROBLEM STATEMENT

We assume optical links with weakly coupled MCFs in SS-FONs [32]. The cores next to each other (called adjacent/neighbor cores) impose XT on each other, and the XT from other cores is not significant [3,13,15,17,18,21,22,33]. Each link has a single MCF in both the directions; however, the proposed work can easily be generalized for multiple fibers per link. The SS-FON operates with a flexible grid of 12.5 GHz granularity. The nodes are equipped with coherent transceivers (TRXs) that support compatible reconfigurable bit rates and various MFs. The TRXs operate at a fixed baud rate of 28 GBaud, and each TRX transmits/receives an optical carrier allocated on three FSs, i.e., 37.5 GHz [13,17,21,33].

The selected candidate MFs and their spectral efficiency determine the supported bit rates by each TRX. If the requested bit rate exceeds the maximum capacity of a single TRX using a particular MF, the request is carried by several optical carriers within one superchannel (SCh). Each SCh is separated from its neighbor SChs by 12.5 GHz guard bands. The general equation to calculate the number of FSs on the kth SP on a route r is given as $\left(\left\lceil \frac{m_i}{(n_t\delta)\eta_r^k} \right\rceil \times n_t + g_b\right)$, and the notations are given in Table 1 below. The spectrum occupied by a TRX is given as $n_t\delta$ GHz. The supported bit rate by each MF is given as $n_t\delta\eta_r^k$ Gb/s. Two challenging and widely accepted core geometries, three-core and seven-core [13], are studied. Furthermore, we study the network performance when spatial continuity is imposed as well as when it is relaxed. Imposed spatial continuity (iSC) means that the same core is assigned to a lightpath on all MCF links on a route, eliminating SDM lane change operation; on the other hand, relaxed spatial continuity (rSC) means that the core indices can be different on different links on the route [34]. A limited number of nodes are assumed to be equipped with 3R regeneration capability. If one or more intermediate node(s) on a route possesses regeneration capabilities, then the route is divided into multiple lightpath segments (LSs) that are separated by regenerators. The connection is only established if the resources are available on all the segments. The use of 3R regenerators may allow for SC and MC. To understand the impact of these, we consider the case when a regenerator allows both SC and MC [the spectrum and modulation conversion (SMC) case] and when SC and MC are not used and the regenerators are used only to mitigate the QoT (i.e., each LS should be shorter than the TR). We call this latter case nSMC (i.e., no spectrum or modulation conversion).

The total XT experienced by a core is the sum of individual average XT contributions from each neighbor. The coupled-power theory-based analytical model to determine mean XT levels in MCF links in [3] is often used in SS-FON studies. Using that model, the mean XT, denoted as XT_μ, can be calculated using

$$\mathrm{XT}_\mu = \frac{N_{\mathrm{AC}} - N_{\mathrm{AC}}\exp(-(N_{\mathrm{AC}}+1)hL)}{1 + N_{\mathrm{AC}}\exp(-(N_{\mathrm{AC}}+1)hL)}, \tag{1}$$

where L is the path length, h is the power-coupling coefficient, and N_{AC} is the number of adjacent cores that are the source of XT in a given core and in a given spectrum band.

In [33], Rottondi *et al.* obtain the TRs, as shown in Tables I and II in [33], for each MF and different values of adjacent lit cores (litcores, for short) by using the modified Gaussian noise (GN) model in [35]. The GN model estimates the XT of weakly coupled MCFs. The authors of [33] assumed two values for average XT between two adjacent cores after a single span of propagation, namely, -25 dB and -40 dB. On the other hand, all the MFs in [33], which are PM-QPSK, PM-8QAM, PM-16QAM, PM-32QAM, and PM-64QAM, can be applied without the need for multi-input multi-output digital signal processing (MIMO DSP) only with $\mathrm{XT} = -40$ dB for a bit error rate (BER) equal to 3.8×10^{-3} [36]. Additionally, the XT thresholds for MIMO DSP-free transmission at $\mathrm{BER} = 3.8 \times 10^{-3}$ were reported in [36]. For instance, the XT thresholds for PM-QPSK and PM-64QAM are -15.6 and -28.1 dB, respectively [36]. Thus, by considering an average XT of -40 dB between two adjacent cores after a single span of propagation, we can ensure that the transmission is MIMO DSP-free for all MFs and number of litcores.

In this paper, we consider an average XT value of -40 dB between two adjacent cores after a single span of propagation [33]. Let γ_d denote the number of allowable litcores for a candidate dth MF. γ_d for an existing connection using MF d on a core determines the allowable occupancy of adjacent cores on the OS. On the other hand, for an incoming connection request, γ_d of a candidate MF d decides whether or not the spectrum can be occupied with this MF based on the occupancy of OsaCs. Thus, a high value of γ_d is desired.

Examples to show the effect of the choice of the MF and core in a seven-core MCF link are shown in Fig. 1. In this paper, we assume five choices of polarization multiplexed (PM) MFs; viz., PM-QPSK ($d = 1$), PM-8QAM ($d = 2$), PM-16QAM ($d = 3$), PM-32QAM ($d = 4$), and PM-64QAM ($d = 5$). Suppose an arriving connection request has two MF choices:

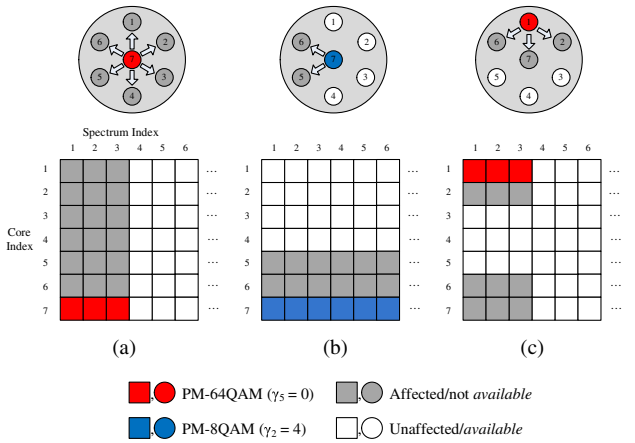

Fig. 1. Effect of the choice of MF based on its XT tolerance for assignment on spectrum utilization in the spatial domain and frequency domain.

(a) PM-64QAM ($d = 5$) with $\gamma_5 = 0$ and the requirement for three FSs, and (b) PM-8QAM ($d = 2$) with $\gamma_2 = 4$ and the requirement for six FSs. As shown in Fig. 1(a), when the PM-64QAM on core 7 is chosen for assignment, OsaCs on all the adjacent cores will not be allowed to be occupied as long as this connection exists in the network. Thus, a total of 21 FSs ($= 3 \times 7$) must be reserved. Similarly, for the PM-8QAM on core 7, a total of 18 FSs ($= 6 \times 3$ FSs) must be reserved, as shown in Fig. 1(b). Thus, although PM-8QAM is less spectrally efficient, it is a better choice than PM-64QAM in this case. However, if core 1 is selected instead of core 7, then only 12 FSs ($= 3 \times 4$) are needed for PM-64QAM, as shown in Fig. 1(c), and this is the better choice now. Clearly, there is a trade-off between spectrum utilization and the corresponding XT levels with the selection of an MF-core pair.

4. PATH PRIORITIES

The RMCSA problem is a complex one, particularly when impairments such as XT are considered; therefore, we decompose it into two separate sub-problems: an offline planning part that selects path priorities and a dynamic MCSA provisioning algorithm. Traffic forecasting can be used to predict the long-term average traffic intensities for different node pairs, and we therefore assume that we are given the dynamic traffic loads on all the routes (i.e., s-d pairs). The path priorities for a route are selected to balance the loads among the multiple paths. We note that these path priorities simply determine the search order of the paths for an arriving connection request. The actual availability of a path is dependent on the network state when a connection request arrives and cannot be known in advance. We explain how path priorities are used to select the path for an arriving connection request in the online resource assignment in the following sections. Path priorities are based on path probabilities (PPs) that optimize the link load. The notations and symbols are defined in Table 1. K SPs for each s-d pair are pre-computed, and an MILP is solved offline to determine the PPs, similar to our previous work in [37]. The SPs are then prioritized from higher to lower PPs for assignment in what we call priority-based path selection (PPS).

The objective (z_{fs}) of the MILP is to minimize the sum of the average link load and maximum link load, as shown in

$$\text{Minimize } z_{\text{fs}} = \frac{1}{L}\sum_{e=1}^{L}\sum_{r=1}^{R}\frac{W_r u_r^e}{F^e C} + \max_e \sum_{r=1}^{R}\frac{W_r u_r^e}{F^e C}. \quad \textbf{(2)}$$

The loads are averaged over the total spectrum on a link e, which is $F^e C$. The probability of selecting the kth SP of route r is denoted as p_r^k, as shown in Eqs. (3a) and (4a), and u_r^e is defined as the spectrum requirement on link e by route r, as shown in Eqs. (3b) and (4b):

Variables:

$$0 \le p_r^k \le 1, \quad \textbf{(3a)}$$

$$0 \le u_r^e \le \left\lfloor \frac{Bw}{\delta} \right\rfloor. \quad \textbf{(3b)}$$

Constraints:

$$\sum_{k=1}^{K} p_r^k = 1, \quad \textbf{(4a)}$$

$$u_r^e = \begin{cases} \sum_{k=1}^{K} R_{r,k}^e p_r^k, & \text{transparent network} \\ \sum_{k=1}^{K}\left(\sum_{s=1}^{G^k} R_{r,k,s}^e\right) p_r^k, & \text{translucent network} \end{cases}. \quad \textbf{(4b)}$$

We assume in this offline calculation that the highest possible MF for the length of the path is used to calculate the number of required FSs. The supporting equations for a translucent network and a TpN are given in Eqs. (6) and (8) and in Eqs. (5) and (7), respectively, which can be found in Table 1. The load distribution on each link varies in translucent networks (based on the presence of a regenerator) and TpNs, and the corresponding equations are given in Eqs. (4b). The calculation of u_r^e includes the calculation of the spectrum requirement by (each segment of) each SP of each route in a transparent (translucent) network. First, the effective spectrum requirement on a (given segment of) a given SP on a given route, denoted as N_r^k (N_r^{k,s_i}), is shown in Eq. (5) [(6)]. Based on traffic distribution, ρ_i is obtained and used to weight the contribution in spectrum utilization by each data rate. Finally, the fraction of utilized spectrum is calculated for each link as shown in Eq. (7) [(8)]. The calculation is done for the SPs that transverse the given link with the help of $A_{r,k}^e$ (A_{r,k,s_i}^e).

We explain the difference between K-SP routing and PPS with an example. Suppose for a route r there are three available SPs, viz. sp_1, sp_2, and sp_3, in increasing order of path length. In K-SP routing, the SPs are considered in increasing order of path length for spectrum assignment, i.e., in the order sp_1, sp_2, and sp_3. Suppose the PPs obtained by solving the MILP are p_r^1, p_r^2, and p_r^3 for sp_1, sp_2, and sp_3. If, for example, $p_r^2 > p_r^1 > p_r^3$, then in PPS, the order of SPs considered for spectrum assignment will be sp_2, sp_1, and sp_3.

Table 1. Symbols and Notations

Symbol	Definition
N	Number of nodes in the network
L	Number of links in the network
e	Arbitrary network link
F^e	Number of fibers on link e
R	Number of routes in the network
r	Arbitrary route
W_r	Load for route r; depends on the traffic pattern; $W_r = 1, \forall\, r$ for uniform traffic
M	Set of connection data rates $\{m_1, m_2, \ldots, m_{\lvert M\rvert}\}$
m_i	ith data rate in Gb/s
ρ_i	Probability that an arbitrary request has rate m_i; $\sum_{i=1}^{\lvert M\rvert} \rho_i = 1$; for uniformly distributed traffic $\rho_i = \frac{1}{\lvert M\rvert}\ \forall i \le \lvert M\rvert$
C	Number of cores per fiber
K	Number of SPs considered for a route
G^k	Number of lightpath segments on the kth SP of route r
k	Arbitrary SP
Bw	Total spectrum available in GHz
δ	Slice width in GHz
$A^e_{r,k}$	$= 1$ if link e is on the kth SP of route r; $= 0$, otherwise
A^e_{r,k,s_i}	$= 1$ if link e is on ith LS s_i on the kth SP of route r; $=\ 0$, otherwise
η^k_r	Spectral efficiency of the selected MF for the kth SP of route r
η^{k,s_i}_r	Spectral efficiency of the selected MF for the ith LS s_i on the kth SP of route r
g_b	Number of FSs used as guard bands
n_t	Number of FSs required for a TRX/carrier
N^k_r	Number of FSs required on the kth SP of route r; $$N^k_r = \sum_{i=1}^{\lvert M\rvert} \rho_i \left(\left\lceil \frac{m_i}{(n_t\delta)\eta^k_r} \right\rceil \times n_t + g_b \right) \quad (5)$$
$N^{s_i,k}_r$	Number of FSs required on the ith LS s_i on the kth SP of route r; $$N^{k,s_i}_r = \sum_{i=1}^{\lvert M\rvert} \rho_i \left(\left\lceil \frac{m_i}{(n_t\delta)\eta^{k,s_i}_r} \right\rceil \times n_t + g_b \right) \quad (6)$$
$R^e_{r,k}$	Fraction of FSs utilized on link e on the kth SP of route r; $$R^e_{r,k} = A^e_{r,k} N^k_r \quad (7)$$
R^e_{r,k,s_i}	Fraction of FSs utilized on link e on the ith LS of the kth SP of route r; $$R^e_{r,k,s_i} = A^e_{r,k,s_i} N^{k,s_i}_r \quad (8)$$

5. NETWORK CAPACITY, CAPACITY LOSS, AND TRIDENTAL COEFFICIENT

In this section, we define several concepts used in TRA for the iSC case and then extend them for the rSC case. We also present an illustrative example to explain the calculations involved. Finally, we explain the changes to be made to TRA for translucent networks to get TaTRA. We call a candidate set of FSs that must be assigned to a connection as a slice window (SW). The aim of TRA is to choose the best SW along with the MF and core to yield the best blocking performance. On SP k of route r (namely, r^k), there are a number of SWs: the first one has a starting FS of 1, the second SW has a starting FS of 2, and so on. The capacity, capacity loss (CL), and tridental coefficient (TC) of a candidate SW are defined as follows.

A. Capacity of a Slice Window

The capacity of the nth SW on r^k for a given MF f_d, denoted by $\upsilon^{k,d}_n$, is the number of cores on the whole path on which the SW can be assigned in the current network state (i.e., before resource assignment for the incoming request). Here, the current network state includes the litcore restriction of the already established connections on the OsaCs. When an SW is assigned to the incoming request on a core with MF f_d, the capacity would decrease by an amount that depends on f_d and its corresponding γ_d for the length of the lightpath. Thus, the remaining capacity of the nth SW on the cth core on r^k using f_d, denoted as $\upsilon'^{k,d}_{n,c}$, is the capacity of the SW if this SW were to be assigned to the incoming request, with the actual value of γ_d of the selected MF f_d and the actual network state at the time the request arrives.

B. Capacity Loss of a Slice Window

The remaining capacity of an SW after the resource assignment of a connection varies based on the selected core and XT tolerance of the selected MF f_d. Thus, each core-MF pair would result in a different value for the remaining capacity, $\upsilon'^{k,d}_{n,c}$. In this paper, we calculate the CL for every SW based on the hypothetical assignment of the core, MF, and SW for the incoming request. The decrease in capacity after the hypothetical provisioning from the capacity before provisioning gives the total CL. If the XT constraints are removed, the CL for any selection of SW for a core on a route is always one, since the spectrum on adjacent cores would not be blocked. However, in SS-FONs, the XT tolerance of the selected MF on a core determines the future occupancy on adjacent cores; thus, the CL can be more than one. Finally, the CL for the nth SW on the cth core on r^k using f_d, denoted as $\psi^{k,d}_{n,c}$, is calculated using

$$\psi^{k,d}_{n,c} = \upsilon^{k,d}_n - \upsilon'^{k,d}_{n,c}. \quad (9)$$

The optimal choice of spectrum is when shared resources in the network are still available for future demands. When an SW on a path is assigned to a request, there also is a CL for the SW on all the overlapping (shared) paths. Thus, we consider the network occupancy by calculating the CL of the same SW on all the shared paths. The CL for the incoming request's path and the shared paths are weighted with the corresponding PPs, which are computed in Section 4, to get the total CL.

Let Z^k be the set of all the shared paths of r^k; $Z^k = i_1, i_2, \ldots, i_z$. The PP of r^k is denoted as p^k_r and of i_z as p_z, which is obtained in Section 4. Suppose that the incoming request has a data rate m and arrived on route r; it is denoted by $\Delta(r, m)$. The number of FSs required to accommodate the data rate m using MF f_d is denoted as β^m_d. We assume a

lightpath tuple, $l_{\Delta(r,m)}(k, c, n, \beta_d^m)$, which represents the nth SW of size β_d^m on the cth core on r^k for request $\Delta(r, m)$. The total CL of $l_{\Delta(r,m)}(k, c, n, \beta_d^m)$ is shown in

$$\psi'(l_{\Delta(r,m)}) = p_r^k \psi^{r\,k,d}_{n,c} + \sum_{z=1}^{|Z^k|} p_z \psi^{i\,z,d}_{n,c}, \tag{10}$$

where $\psi^{r\,k,d}_{n,c}$ is the CL ($\psi^{k,d}_{n,c}$) on r^k and $\psi^{i\,z,d}_{n,c}$ is the CL ($\psi^{k,d}_{n,c}$) on the zth shared path i_z ($i_z \in Z^k$).

In the rSC case, the core selection on each link is independent. Thus, the CL calculation is performed separately for each link. The final CL of an SW on a route is the maximum (over all links on the path) of the minimum CL (over all cores on a link) on a route. Let us say that the set of cores is denoted as Θ and the set of links as E. The CL of the nth SW on the cth core on the eth link on r^k using f_d, denoted as $\psi^{k,e,d}_{n,c}$, contributes to the final CL, which is independent of the core index and is denoted as $\psi^{k,d}_n$; this is shown in

$$\psi^{k,d}_n = \max_{e\in E} \min_{c\in\Theta} \psi^{k,e,d}_{n,c}. \tag{11}$$

The final CL of an SW is given in

$$\psi'(l_{\Delta(r,m)}) = p_r^k \psi^{r\,k,d}_{n} + \sum_{z=1}^{|Z^k|} p_z \psi^{i\,z,d}_{n}. \tag{12}$$

C. Tridental Coefficient

The CL is a measure of how much future capacity is lost because of assigning a candidate SW with a particular core-MF pair to the incoming request. Apart from loss in capacity, the selection of MF, core, and SW also affects the amount of required spectrum and fragmentation levels. We could penalize the MFs that demand higher spectrum and use the first-fit policy of lower-indexed SWs, which can reduce fragmentation. To capture these effects, we consider two more factors besides CL in the definition of a TC.

The TC of $l_{\Delta(r,m)}$ is defined as the sum of the normalized values of the CL, the size of required SW in terms of the number of FSs, and the starting index of the SW. It is denoted as $\Psi(l_{\Delta(r,m)})$ and is given in

$$\Psi(l_{\Delta(r,m)}) = \frac{\psi'(l_{\Delta(r,m)})}{\max\psi'(l_{\Delta(r,m)})} + \frac{\beta_d^m}{\beta_1^m} + \frac{n}{S-\beta_d^m+1}. \tag{13}$$

The normalization is done using the respective maximum values, viz., the maximum possible CL denoted by $\max \psi'(l_{\Delta(r,m)})$ as shown in

$$\max\psi'(l_{\Delta(r,m)}) = \left(p_r^k + \sum_{z=0}^{|Z^k|} p_z\right) \times C; \tag{14}$$

the largest possible demand size of the data rate m denoted as β_1^m; and the highest possible index of an SW, equal to $S-\beta_d^m+1$. $\max\psi'(l_{\Delta(r,m)})$ is obtained using PPs and assuming maximum CL, which is equal to C, on the main route and shared paths. The consideration of normalized CL ensures that the least lossy SW is selected. The normalized demand size ensures that low spectrum utilization is favored. Finally, the normalized index of the SW encourages the first-fit behavior, which decreases fragmentation. Experiments suggest that normalization over maximum value yields better results than normalizing over maximum and minimum values [6].

D. Illustrative Example

In this section, we present an example to explain the calculation of CL for the iSC and rSC cases for a TpN. We also discuss the changes in the computational approach for a translucent network.

We illustrate the calculations of CL and TC for the first SW ($n=1$) on core 1 of a 7-core fiber for two different candidate MFs for the iSC and rSC cases with the help of an example shown in Fig. 2 and Table I from [33]. Let us consider a portion of a network with six nodes, as shown in Fig. 2(a). Here, v_i denotes the ith node/vertex, l_j denotes the jth link, and the corresponding occupancy of cores is shown on each link. In the TpN scenario, suppose that the first SP ($k=1$) between v_1 and v_3 has the highest PP and is shown as r^1 ($v_1-v_2-v_3$). The corresponding shared paths in $Z^1=\{i_1, i_2\}$ are shown as i_1 ($v_1-v_2-v_3-v_4$) and i_2 ($v_5-v_2-v_3-v_6$). D is the set of MFs $\{f_1, f_2, \ldots, f_{|D|}\}$. In this example, we assume that $|D|=5$ and use PM-32QAM (f_4) and PM-8QAM (f_2) for the explanation. We use Table I from [33] to get γ_d of both the MFs. Table I from [33] reports the TRs calculated for the combination of MF and number of adjacent litcores (γ_d) for the TRX baud rate of 28 GBaud and average XT between two adjacent cores after a single span of propagation (XT^{sp}) of -25 dB. The number of litcores varies from 0 to 6 in a 7-core fiber; thus TRs are given for each MF for $\gamma_d=0, \ldots, 6$. The corresponding value of γ_d for which the TR of the dth MF is greater than or equal to the path length is chosen for a given MF on this path.

Assume that r^1, i_1, and i_2 have PPs of 0.6; i.e., $p_r^1 = p_1 = p_2 = 0.6$. Assume that, out of $S=320$ FSs, the first 7 FSs are occupied by a connection that uses PM-QPSK (f_1) with $\gamma_1=6$ on cores 3 and 5 on link l_2 and on core 4 on link l_4, and the first 4 FSs are occupied by a connection that uses PM-32QAM (f_4) with $\gamma_4=0$ on core 4 on link l_5. The FSs on the rest of the cores on all the links are free. Suppose a connection request of 200 Gb/s arrives on r, and the length of r^1 is 150 km, which requires $\beta_4^m=4$ FSs, $\beta_2^m=7$ FSs, and $\beta_1^m=7$ FSs when PM-32QAM (f_4), PM-8QAM (f_2), and PM-QPSK (f_1) are chosen. The first SW ($n=1$) for PM-32QAM is of the size β_4^mFSs and for PM-8QAM is of the size β_2^m. For the iSC case, an SW is considered to be free if it is available on the same core on all the links. The OS of respective sizes is free on cores 1, 2, 4, 6, and 7; i.e., the capacity before any assignment for both the selections is 5 (i.e., $\upsilon_1^{1,4}=\upsilon_1^{1,2}=5$). The hypothetical assignment is done to see the remaining capacity after a selection of the MF. Starting from the highest MF [i.e., PM-32QAM (f_4)], the hypothetical assignment is done on core 1, as shown in Fig. 2(b). From Table I from [33] for PM-32QAM, because the first TR, searched from the bottom to the top, at $\gamma_2=0$ (550 km) is higher than the path length (150 km), γ_4 is set to 0. This

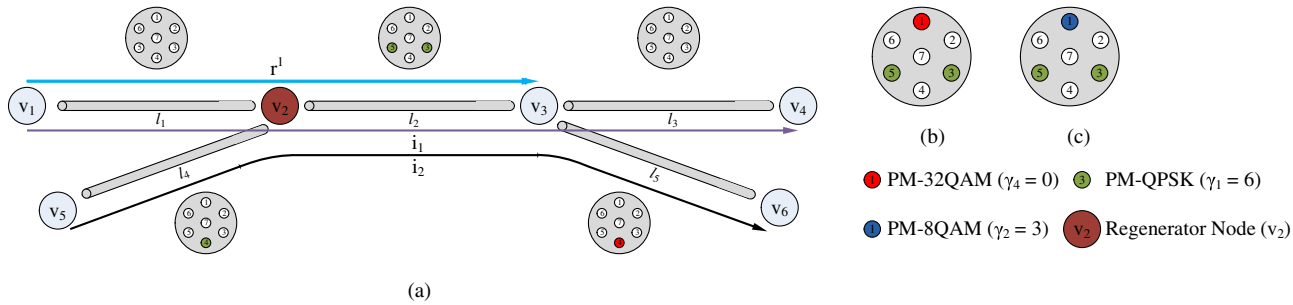

Fig. 2. Illustration of the effect of the presence of a regenerator on CL for the iSC and rSC cases.

means that, based on the XT tolerance of PM-32QAM, if assigned for the current connection on core 1, the connection will not allow adjacent cores 2, 6, and 7 to be assigned to future requests on the OS as long as it exists in the network. Thus, the OS on only core 4 will be available for future connections, which means that the capacity after hypothetical assignment with PM-32QAM is 1; i.e., $\upsilon'^{1,4}_{1,1} = 1$. Thus, using Eq. (9), the CL $\psi^{r\,1,4}_{1,1}$ in this case is $\upsilon^{1,4}_{1} - \upsilon'^{1,4}_{1,1} = 5 - 1 = 4$. Similarly, the CL on i_1 is 4; i.e., $\psi^{i\,1,4}_{1,1} = 4$ as $\upsilon^{1,4}_{1} = 5$ and $\upsilon'^{1,4}_{1,1} = 1$. In the case of i_2, the existing connection at core 4 on link l_5 blocks the OS of size 4 ($= \beta^m_4$) on cores 3, 5, and 7. Thus, SW on only cores 1, 2, and 6 are allowed to be occupied on i_2. Thus, the capacity before is 3, i.e., $\psi^{i\,1,4}_{1,1} = 3$, and the capacity after becomes 0, i.e., $\upsilon'^{1,4}_{1,1} = 0$; thus, CL is $\psi^{i\,1,4}_{1,1} = 3$. Using Eq. (10), the total CL ($\psi'(l_{\Delta(r,m)})$) with PM-32QAM is $0.6 \times 4 + 0.6 \times 4 + 0.6 \times 3 = 6.6$. The maximum value of the total CL ($\max \psi'(l_{\Delta(r,m)})$) is 12.6 using Eq. (14). Hence, the TC of the first SW with PM-32QAM ($\Psi(l_{\Delta(r,m)})$), by substituting the values in Eq. (13), is $\frac{6.6}{12.6} + \frac{4}{7} + \frac{1}{320-4+1} = 1.0984$. Similarly, we can calculate the CL for hypothetical assignment of PM-8QAM on core 1, as shown in Fig. 2(c). For the first SW of size β^m_2 with PM-8QAM, from Table I from [33], we get $\gamma_2 = 3$; i.e., if assigned, it will allow the OS to occupy on the adjacent cores 2, 6, and 7 by future requests as long as it remains in the network. So, the OS on cores 2, 4, 6, and 7 on r^1 will be available for future connections. The capacity after hypothetical assignment with PM-8QAM is 4, i.e., $\upsilon'^{1,2}_{1,1} = 4$. The CL $\psi^{r\,1,2}_{1,1}$ in this case is $\upsilon^{1,2}_{1} - \upsilon'^{1,2}_{1,1} = 5 - 4 = 1$. Similarly, the CL at i_1 is 1, i.e., $\psi^{i\,1,2}_{1,1} = 1$ ($= 5 - 4$), and the CL at i_2 is $\psi^{i\,1,2}_{1,1} = 1$ ($= 3 - 2$, after considering the effect of PM-32QAM on l_5). The total CL ($\psi'(l_{\Delta(r,m)})$) with PM-8QAM is $0.6 \times 1 + 0.6 \times 1 + 0.6 \times 1 = 1.8$. Using Eq. (13), the TC of the first SW with PM-8QAM ($\Psi(l_{\Delta(r,m)})$) is $\frac{1.8}{12.6} + \frac{7}{7} + \frac{1}{320-7+1} = 1.1460$.

For the rSC case, the scenario changes because the CL is computed separately for each link. The CL of the first SW on l_1 for PM-32QAM values for all the outer cores is $\psi^{1,1,4}_{1,c} = 4$ and on the central core is $\psi^{1,1,4}_{1,7} = 7$. On link l_2, only core 1 can accommodate PM-32QAM as $\gamma^5 = 0$; thus, the CL value, $\psi^{1,2,4}_{1,1}$, of core 1 is 4 and for rest of the cores is ∞. Thus, for a given SW, core 1 on l_1 and core 1 on l_2 are selected because they offer the smallest CL compared to other cores on the corresponding links. The final CL of an SW on r^1, $\psi^{r\,1,4}_{1}$, is 4, as per Eq. (11). Similarly, shared path i_1 has the CL, $\psi^{i\,1,4}_{1}$, of 4 ($= \max\{4, 4, 4\}$), and i_2 has the CL, $\psi^{i\,2,4}_{1}$, of 4 ($= \max\{4, 4, 2\}$). Using Eq. (12), the total CL is $\psi'(l_{\Delta(r,m)}) = 0.6 \times 4 + 0.6 \times 4 + 0.6 \times 4 = 7.2$. The TC becomes 1.1460 ($= \frac{7.2}{12.6} + \frac{4}{7} + \frac{1}{320-4+1}$) using Eq. (13). Similarly the TC for a given SW when PM-8QAM is chosen is also 1.1460 ($= \frac{1.8}{12.6} + \frac{7}{7} + \frac{1}{320-7+1}$). In the case of a tie, the first choice is selected.

Now, suppose node v_2 has regeneration capability. r^1 gets broken down into two LSs s_1 and s_2, denoted as $r^1_{s_1}$ ($v_1 - v_2$) and $r^1_{s_2}$ ($v_2 - v_3$). Similarly, i_1 is divided into i_{1,s_1} ($v_1 - v_2$) and i_{1,s_2} ($v_2 - v_3 - v_4$), and i_2 is divided into i_{2,s_1} ($v_5 - v_2$) and i_{2,s_2} ($v_2 - v_3 - v_6$). Thus, $Z^1 = \{i_1, i_2\}$ in the case of TpN gets divided as $Z^1_{s_1} = \{i_{1,s_1}\}$ for $r^1_{s_1}$ and $Z^1_{s_2} = \{i_{1,s_2}, i_{2,s_2}\}$ for $r^1_{s_2}$ in the case of a translucent network. On the other hand, the CL is calculated for r^1 for the TpN, and the CL is calculated separately for both $r^1_{s_1}$ and $r^1_{s_2}$ for the translucent network.

6. TRIDENTAL RESOURCE ASSIGNMENT AND TRANSLUCENCY-AWARE TRIDENTAL RESOURCE ASSIGNMENT

We first describe our proposed algorithm, TaTRA, for SMC (the case with SC and MC at regenerator nodes) and then show how it is modified for nSMC and as TRA for TpNs. First, we define an available SW (which is a candidate SW for assignment).

Definition 6.1: Available Slice Window (iSC Case). An SW of size β^m_d starting at FS n is called an *available* SW for assignment to a connection request with a data rate m on route r, denoted as $\Delta(r, m)$, using MF f_d on a *core c on all the links* on a given SP of route $r \Leftrightarrow$ all the FSs from index n to $n + \beta^m_d - 1$, on *core c on all the links* of given SP of route r, a) are free, i.e., not assigned to any other connection; b) can accommodate $\Delta(r, m)$ without affecting ongoing connections on OsaCs of *core c* on all the links; and c) can accommodate $\Delta(r, m)$ based on XT sensitivity of MF f_d.

In the iSC case, an FS on a core is considered as free/available only if it is free on the same core index on all the links on the path. The second condition is satisfied by checking the maximum value of allowable γ_d over all the overlapping FSs in an SW on each of the adjacent cores on all the links. In other

words, the ongoing connections on the adjacent cores should allow the new connection to be placed on the current core. In the third condition, the maximum value of occupied cores over all the FSs in an SW over all the links should be less than or equal to the obtained γ_d. For the rSC case, the definition above holds true by replacing the italic statement with "given core on each link."

An SP is broken down into one or more LSs based on the presence of a regenerator on the intermediate nodes, as explained in Section 5.D, and based on the regenerator's capability to handle MC and SC, as well as network performance changes. SC allows us to avoid spectrum continuity constraints. In an SMC case of a translucent network, SC and MC are allowed. On the other hand, in an nSMC case of a translucent network, SC and MC are prohibited, meaning that the same MF and spectrum have to be selected on all the LSs. In this section, we explain the working principle of the TaTRA algorithm for SMC. We then explain the changes to be made in the algorithm of TaTRA for SMC to get TRA and TaTRA for nSMC because these are special cases.

All the possible SWs for data rate m using MF f_d on all the cores are stored in set B_d^m. The SWs are stored starting from the lowest index of SW on all the cores in increasing order of the core index before moving to the next SW. For data rate m, H^m is the set of all B_d^m sets for all MFs. The SW of index n on core c in B_d^m is denoted by $b_{n,c}^{m,d}$. For the data rate m, V^m is the set of β_d^m for all MFs. Based on the β_d^m value, if two or more MFs have the same β_d^m then only the lowest among them is considered for assignment. Such sorted MFs are stored in D^m. This assures the selection of higher γ_d with the same spectrum utilization.

The selection of a path, MF, core, and SW by TaTRA-SMC for a lightpath is explained in Algorithm 1. For simplicity, we assume that the SPs are sorted and renumbered as per the corresponding value of PP p_r^k from highest $(k=1)$ to lowest $(k=K)$ in set $P(r)$. The TR of MF f_d for the corresponding value of γ_d is denoted as T_d^γ. The best lightpath $l_{\Delta(c,m)}^*(k^*, c^*, n^*, \beta^*)$, its corresponding TC, the SP with the highest PP, and the number of processed LSs, denoted as PLS, are initialized in Line 1. Assume that the kth SP is broken down into one or more LSs that are stored in Ω_r^k, where the ith LS is denoted as s_i. Here, the desired path index, set of core indexes, set of indexes of SW, and set of demand sizes are denoted by k^*, c^*, n^*, and β^* on the whole route. These sets store the data for each link as for the rSC case and the SMC case; each link can have different values of n, β_d^m, and c if all the intermediate nodes have regenerators. In Line 2, the algorithm continues until either the best lightpath is obtained or the search over all the SPs is completed. In Line 3, the search is done for all the LSs on a kth SP in Ω_r^k. In Line 4, the search is initiated for MFs in D^m whose maximum TR [i.e., TR without the consideration of XT at $\gamma_d = 0$ (T_d^0)] is higher than the length of s_i, denoted as w^{s_i}. In Line 5, the γ_d for which the TR value T_d^γ is greater than w^{s_i} is obtained. In Line 6, the actual and largest sizes of the SW are obtained. In Line 7, a loop iterates over all the choices of SWs in B_d^m. The candidate LS $l_{\Delta(r,m)}^{k,s_i}$ is initiated in Line 8. If the SW is available as per Definition 6.1 and the iSC/rSC constraint in Line 9, the TC is calculated for the current SW $b_{n,c}^{m,d}$ on the LS in Line 10. The

Algorithm 1. TaTRA-SMC Algorithm

Input: Network topology, $\Delta(r, m)$, set of SPs $P(r)$, their PPs p_r^k, set of LSs Ω_r^k and their lengths w^{s_i} and, D^m, V^m, H^m, S
Output: $l_{\Delta(r,m)}^*(k^*, c^*, n^*, \beta^*)$
1. Initialize: $l_{\Delta(r,m)}^* \leftarrow \emptyset$, $\Psi(l_{\Delta(r,m)}^*) \leftarrow \infty$, $k \leftarrow 1$, PLS $\leftarrow 0$
2. **while** $l_{\Delta(r,m)}^* = \emptyset \wedge k \neq K$ **do**
3. **for all** $s_i \in \Omega_r^k$, $\Omega_r^k \in P(r)$ **do**
4. **for all** $(f_d \in D^m \wedge T_d^0 \geq w^{s_i})$ **do**
5. Get litcore $\gamma_d \leftarrow \gamma$ for which $T_d^\gamma \geq w^{s_i}$
6. Get β_d^m and β_1^m from V^m
7. **for all** $(b_{n,c}^{m,d} \in B_d^m; B_d^m \in H^m) \wedge (n \leq (S - \beta_d^m + 1))$ **do**
8. Get candidate lightpath $l_{\Delta(r,m)}^{k,s_i} \leftarrow (s_i, c, n, \beta_d^m)$
9. **if** SW is available as per iSC/rSC constraint (see Definition 6.1) **then**
10. Calculate TC $\Psi(l_{\Delta(r,m)}^{k,s_i})$ of $b_{n,c}^{m,d}$ SW
11. Get corresponding core index(es) on LS
12. **if** iSC constraint is active **then**
13. Get $c^{s_i} \leftarrow \{c'[i] = c | i \leq |E^{k,s_i}|\}$
14. **else if** rSC constraint is active **then**
15. $c^{s_i} \leftarrow \{c_1, \ldots, c_{|E^{k,s_i}|}\}$
16. **end if**
17. **if** $\Psi(l_{\Delta(r,m)}^{k,s_i}) < \Psi(l_{\Delta(r,m)}^{*k,s_i})$ **then**
18. $l_{\Delta(r,m)}^{*k,s_i} \leftarrow l_{\Delta(r,m)}^{k,s_i}$, $c^{*s_i} \leftarrow c^{s_i}$, $n^{*s_i} \leftarrow n$, $\beta^{*s_i} \leftarrow \beta_d^m$, PLS $\leftarrow$ PLS $+ 1$
19. **end if**
20. **end if**
21. **end for**
22. **end for**
23. **end for**
24. **if** PLS $= |\Omega_r^k|$ **then**
25. $l_{\Delta(r,m)}^* \leftarrow \{l_{\Delta(r,m)}^{*k,s_i} | \forall s_i \in \Omega_r^k\}$, $c^* \leftarrow \{c^{*s_i} | \forall s_i \in \Omega_r^k\}$, $n^* \leftarrow \{n^{*s_i} | \forall s_i \in \Omega_r^k\}$, $\beta^* \leftarrow \{\beta^{*s_i} | \forall s_i \in \Omega_r^k\}$, $k^* \leftarrow k$
26. **break**
27. **else**
28. $k \leftarrow k + 1$, PLS $\leftarrow 0$
29. **end if**
30. **end while**

corresponding cores that are obtained while calculating the TC for the iSC/rSC constraint are stored in c^{s_i} in Lines 11–16, as explained in Section 5.D. In Lines 17–19, the information of the SW that offers the least value of the TC is stored as the desired LS $l_{\Delta(r,m)}^{*k,s_i}$. In Line 24, the algorithm checks whether the SW is available on all the LSs on the kth SP. If available, the information of the selected resources of all the LSs and the index of the kth SP are stored in desired optimal lightpath $l_{\Delta(r,m)}^*$ and k^* in Line 25 and then the algorithm stops the search. Otherwise, the algorithm continues with the next SP in Lines 27–29. Finally, after all the SWs on all the cores on the whole path are processed, the optimal lightpath $l_{\Delta(r,m)}^*$ is selected for a given connection, and the network resources are assigned accordingly to the connection request. If an SW is not found on all the SPs (i.e., $l_{\Delta(r,m)}^* = \emptyset$), the request is rejected.

In the case of nSMC, the value of w_{s_i} is set to the length of the longest LS on the kth SP because MC is not allowed. Thus, the same MF and β_d^m are selected for all the LSs on the SP in Line 4. In addition, because no SC is allowed, the index of the SW must be the same on all the LSs on the SP. To achieve

that, the information in Line 3 comes after the information in Line 7. In the case of a TpN, the MF is chosen based on the path length of the SP. Thus, there is no change in the algorithm because the number of LSs will always be 1, i.e., the complete SP.

The use of the CL for the selection of the MF, core, and spectrum varies for the iSC and rSC cases. In the iSC case, the CL for each core is distinct from the CLs of other cores but is constant on the whole path for the selected MF-SW pair. The CL is calculated for those cores on which the SW is available on the main route and shared paths. Thus, the selection of an SW on a particular core on the main route actually contributes to the CL of the shared routes. However, in the rSC case, the core on each link can be different, and the selection of a core on a particular link is independent of the core selection on any other link. Thus, shared paths cannot directly impact core selection, but only the selection of an SW. Thus, the CL of an SW on a particular core only on the main route contributes toward the selection of the core. The CL introduced by the shared paths contributes toward the SW selection and thus indirectly selects the core. We analyze the computational time complexity of Algorithm 1. For an incoming connection request between two nodes in the network, there are K SPs with a maximum of L possible links per path. The TC is calculated for all the SWs in B_d^m for each MF. The size of an SW can vary from 1 to S. Due to continuity and contiguity constraints, all the links are searched for each SW. The time complexity of checking if a candidate SW is *available* involves satisfying the three conditions in Definition 6.1. In an SDM-EON, the combined complexity of satisfying the three conditions is $O(LSC)$. The time complexity of the entire algorithm can then be shown to be $O(K|D||B_d^m|LSC)$.

7. SIMULATION RESULTS

We now present simulation results that compare TRA and TaTRA with several other algorithms for a variety of scenarios. We use two practical topologies: generic German (DT) and European (EURO), which are shown in Fig. 3, which is used from [38]. The spectrum of 4 THz ($Bw = 4000$) is considered on each link with each slice of 12.5 GHz ($\delta = 12.5$); i.e., 320 FSs ($S = 320$). A Poisson connection arrival process with an exponentially distributed holding time of 1 (arbitrary time unit) is assumed. The Erlang loads were chosen so that the BBP values generally range between 10^{-5} and 10^{-1}. The load is kept the same for the SMC and nSMC cases of translucent networks for direct comparison. A total of 100,000 requests are generated per trial (excluding 10,000 warm-up requests to bring the network to steady-state). A total of 95% confidence intervals are obtained for 10 trials in each experiment. The data rates are uniformly distributed between 40 and 400 Gb/s with a granularity of 40 Gb/s. We use three SPs between every s-d pair ($K = 3$). A total of five MFs ($|D| = 5$), i.e., f_1 to f_5, are used, viz., PM-QPSK ($\eta_r^k = 2.96$), PM-8QAM ($\eta_r^k = 4.44$), PM-16QAM ($\eta_r^k = 5.92$), PM-32QAM ($\eta_r^k = 7.4$), and PM-64QAM ($\eta_r^k = 8.88$) [17,33]. The supported bit rates for each MF by a TRX carrier are, respectively, 111 Gb/s, 166.5 Gb/s, 222 Gb/s, 277.5 Gb/s, and 333 Gb/s. The TR model for each MF with the average XT between two adjacent cores after a single span of propagation of −40 dB with 28 GBaud TRX with the span length of 50 km is used from [33]. We assume that in translucent networks, 20%–30% of the nodes have regeneration capabilities (three nodes in DT and five in EURO) and these nodes are selected in descending order of nodal degree. Note that the focus of this paper is the evaluation of RMCSA algorithms; evaluation of regenerator placement policies is out of the scope of this paper.

We compare the performance of the proposed algorithms with a baseline XT-avoid approach (XA) [15], worst case XT approach (WC) [11,13,15], XT-aware first-fit algorithm (xtFF) [15], and two algorithms from the literature, KCAP [30] and P-XT [13]. We also compare the performance of the previous version of TRA, published in [6] and called predecessor TRA (pTRA), for TpNs. K-SP routing is used with these algorithms, while PPS is used with TRA and TaTRA. XA chooses the spectrum such that there is no occupancy on OsaCs. In the WC algorithm, the MFs are selected considering the worst-case XT scenario and thus the XT levels automatically remain below the maximum allowable XT. xtFF chooses the highest MF and the first available SW for assignment. KCAP is a path-core priority-based core and spectrum assignment algorithm. The cores are divided into groups and path-core pairs are searched in increasing order of the required number of FSs on the pair based on the TR model using the worst-case XT scenario; i.e., all adjacent cores of a given core are assumed to be lit regardless of how many are actually lit. P-XT does an XT-aware spectrum assignment with an exhaustive search on all the routes. The spectrum available on the lowest index among the ones available on all the path-core pairs is selected. All the algorithms are compared for the same parameters, and especially for the same XT^{sp} and TR model. KCAP and P-XT are not designed for the rSC case, and P-XT is not available for translucent networks.

As discussed in Section 6, the TpN and the nSMC case of a translucent network (nSMC-TlN) are special cases of the SMC case of the translucent network (SMC-TlN). Thus, in Fig. 4, we first present the results for four scenarios for SMC-TlN and present a result for a scenario of $XT^{sp} = -40$ dB and number of cores $C = 7$ for nSMC-TlN and a TpN. In all the scenarios of SMC-TlN, TaTRA-iSC and TaTRA-rSC perform better than the baseline algorithms. In addition, the baseline algorithms are not consistently better or worse than the other baseline algorithms. For instance, xtFF is better than KCAP when $XT^{sp} = -40$ dB and $C = 7$, but KCAP outperforms xtFF by

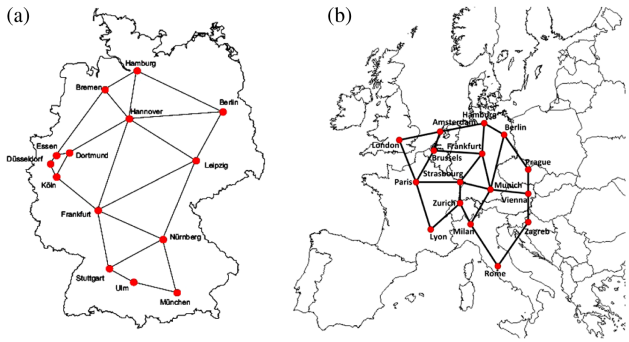

Fig. 3. Network topologies: (a) DT (12 nodes) and (b) EURO (16 nodes) [38].

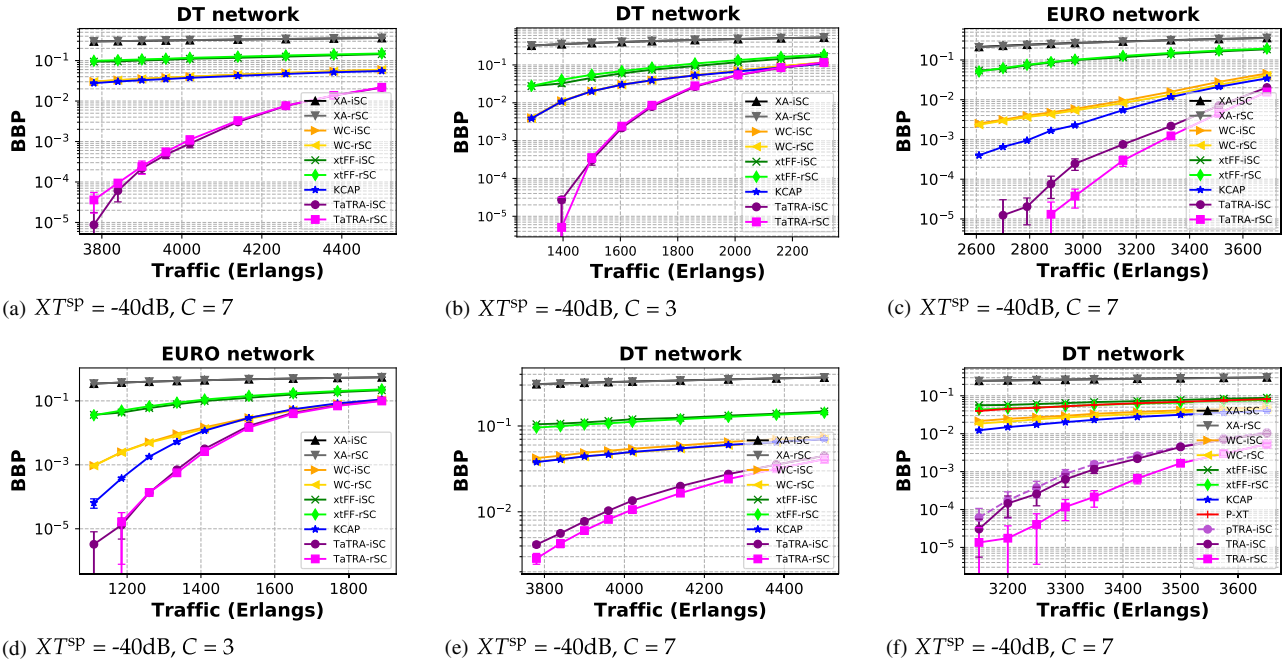

(a) XT^{sp} = -40dB, $C = 7$ (b) XT^{sp} = -40dB, $C = 3$ (c) XT^{sp} = -40dB, $C = 7$

(d) XT^{sp} = -40dB, $C = 3$ (e) XT^{sp} = -40dB, $C = 7$ (f) XT^{sp} = -40dB, $C = 7$

Fig. 4. Variation in BBP with respect to traffic for all the pairs of XT^{sp} and C values for (a)–(d) SMC-TlN, (e) nSMC-TlN, and (f) TpN.

a small margin when $XT^{sp} = -40$ dB and $C = 3$ because of selection of spectrum-efficient MFs due to the TR model on cores with a diverse number of adjacent cores. The same pattern is observed in EURO but with a huge difference in BBP performance of xtFF and KCAP. The difference in performance intensifies from DT to EURO because of larger path lengths and larger TRs offered by $XT^{sp} = -40$ dB, which improves the path-core sorting. In addition, the larger path lengths in the EURO cause decreased use of high/medium spectrum-efficient but XT-sensitive MFs because of the worst-case XT model for a given core assumed by KCAP.

KCAP and WC perform similarly because both have a similar pattern of selection of MFs based on the worst-case XT scenario, but the difference lies in the sorting of path-core pairs in KCAP. When XT^{sp} is -40 dB, KCAP (and WC) perform better due to better utilization of higher values of TRs and corresponding γ_d in the selection of MFs. XA is a simple algorithm and performs comparatively better when the XT^{sp} is more restrictive, as shown in Figs. 4(a) and 4(c), whereas other algorithms suffer due to strict XT restrictions. One would normally expect that relaxing core continuity would improve performance. However, we observe that the performance slightly deteriorates with rSC in some cases, e.g., in the DT topology, as shown in Fig. 4(a). This is because some higher-hop connections may be accepted due to rSC, causing increased XT to other connections; the difference in performance depends upon the RMCSA algorithm. The bigger performance difference of algorithms for $C = 3$ than for $C = 7$ is also because of the absence in the three-core fiber of a central core, which dominates the occupancy of the other cores, as explained in Section 3. It is also observed that the load supported by the DT topology is much higher than that supported by the EURO topology. This is because the EURO topology has higher path lengths, which causes either lower MFs be selected more often and increases spectrum usage, or higher MFs with lower values of γ^d to be selected, thereby increasing spectrum blocking, as explained in Fig. 1.

A similar pattern of performance difference is observed for nSMC-TlN and TpNs compared to SMC-TlN. A direct comparison between the performance of algorithms in SMC-TlN, nSMC-TlN, and TpNs can be made from Figs. 4(a), 4(e), and 4(f). The BBP is higher for the nSMC case than the SMC case for the same load as the MFs are selected based on the length of the largest segment, and continuity and contiguity constraints are imposed. However, there is a similarity between SMC-TlN and TpNs in terms of independently handling the LSs on the SP. Similarly, without regeneration capabilities, the BBP increases in TpNs. These differences in the performance of the same algorithms for SMC-TlN, nSMC-TlN, and TpNs are due to a change in the selection pattern of MFs due to different lengths of segments/paths. In TpNs, pTRA has a slightly worse performance than TRA because TRA uses a different approach for normalization of the required spectrum and spectrum index. The change in TC results in the selection of different core-MF-spectrum combinations, as can be seen in Figs. 5(b) and 6(b).

The performance gains of TaTRA in SMC-TlN and TRA in TpNs over the rest of the algorithms are similar. On the other hand, when the largest length of the LS is chosen to select the MF for all the LSs on an SP in nSMC-TlN, the theoretical length of the SP changes to the length of the largest LS. Thus, the actual topology gets converted into a shrunken version of the same topology, which affects the performance. This explains the variation in performance gains of the proposed algorithm over the other algorithms for nSMC-TlN compared to SMC-TlN and TpNs. Note that the path length of a route/LS alters the selection of MFs and thus affects the spectrum-XT trade-off. TRA and TaTRA balance this trade-off

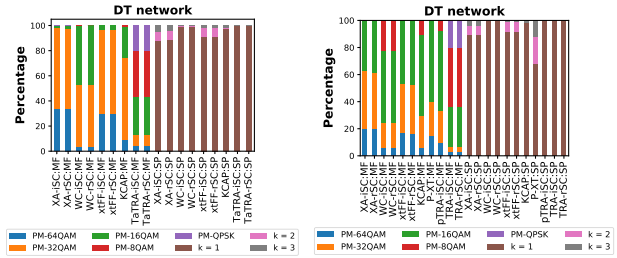

(a) XT^{sp} = -40dB, $C = 7$ (b) XT^{sp} = -40dB, $C = 7$

Fig. 5. Distribution of utilized MFs and SPs for different XT^{sp} values for both the topologies for (a) SMC-TlN and (b) a TpN.

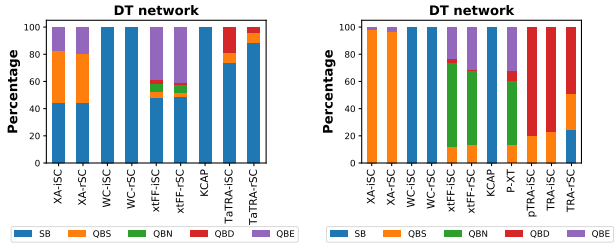

(a) XT^{sp} = -40dB, $C = 7$ (b) XT^{sp} = -40dB, $C = 7$

Fig. 6. Distribution of types of blocking for XT^{sp} and $C = 7$ for the DT topology for (a) SMC-TlN and (b) a TpN.

well and provide better performance for all the scenarios and cases.

It can naively be argued that the selection of higher MFs should be promoted so that the increased remaining spectrum may help in the acceptance of future connections. However, our experiments show that the MFs, which offer a better trade-off between spectrum utilization and XT based on the current XT^{sp} value and core type, are the better choice. To explain this, we present the distribution of utilized MFs and indexes of SPs in Fig. 5. The first set of nine bars in Fig. 5(a) and ten bars in Fig. 5(b) for each algorithm show the % utilization of MFs, mentioned as ":MF," and the second set of bars indicates the % utilization of SPs, mentioned as ":SP." We observe that the algorithms that select the MFs that are either low (favoring XT) or high (favoring spectrum utilization), such as xtFF, KCAP, and WC, have a worse performance than algorithms that select the MF based on balancing the spectrum-XT tradeoff (TaTRA and TRA). P-XT has a better pattern of selection of MFs; however, its performance suffers due to its spectrum selection process. The selection of PM-QPSK is reduced and the PM-QAM is increased in pTRA compared to TRA since the older TC used normalization of spectrum leading to favoring low spectrum occupying MFs. Although the selection of MFs looks different, the performance difference between pTRA and TRA is not huge, as can be seen in Fig. 4(f), which shows that there can be another combination of the selection of MFs to get better performance and both the versions of TRA can achieve it. In addition, pTRA, TRA, and TaTRA choose only the first path ($k = 1$), which is unlike other algorithms that are unable to find the available SW on the first SP due to their previous resource selections. In other words, if the number of SPs per route were restricted to one, then the performance of pTRA, TRA, and TaTRA would remain unchanged, whereas the other algorithms would experience higher bandwidth blocking. The optimal utilization of SPs is an outcome of offline planning to balance the load in the network and dynamic resource selection to make the resources available for the future.

A connection request may be blocked for a variety of reasons. The distribution of blocking types for the highest load is shown in Fig. 6. The available SW satisfies the spectrum availability constraint (SA) (i.e., it is free), the self-QoT constraint (QS) (i.e., it can accommodate the current connection), and the neighbor's QoT constraint (QN) (i.e., it does not affect ongoing connections on the OS). A connection request gets blocked if at least one constraint is not satisfied.

Table 2. Types of Blocking

	Status of Spectrum		
SA	**QS**	**QN**	**Type**
0	×	×	SB
1	0	1	QBS
1	1	0	QBN
1	0	0	QBD
1	1	1	QBE

The types of blocking can be divided into five subcategories, as shown in Table 2. If the constraint is satisfied, it is denoted as 1; otherwise it is denoted as 0. When the SA is 0, the QS and QN do not matter and are denoted as ×. Suppose there are exactly 10 candidate SWs. If none of them are free (i.e., SA = 0∀ SWs), then this is considered to be spectrum blocking (SB). If all 10 SWs are free (i.e., SA = 1), there are several scenarios: (a) if none of them satisfy the self-QoT constraint, but all of them satisfy the neighbor's QoT constraint, then we call this self-QoT blocking (QBS); (b) if all of them satisfy the self-QoT constraint, but none of them satisfy the neighbor's QoT constraint, then we call this neighbor's-QoT blocking (QBN); (c) if none of them satisfy the self-QoT constraint or neighbor's QoT constraint, then we call this dual-QoT blocking (QBD); or (d) if we suppose that x (s.t. $0 < x < 10$) SWs do not satisfy the self-QoT constraint but satisfy the neighbor's QoT constraint (i.e., QS = 0 and QN = 1, and the remaining $10 - x$ SWs are marked as QS = 1 and QN = 0), then we call this either-QoT blocking (QBE), because the blocking is difficult to classify as QBS or QBN.

A direct comparison between blocking types and BBP performance can be done between Figs. 6(a) and 4(a) and between Figs. 6(b) and 4(f) for the DT topology. A higher QBS means that the algorithm efficiently packs the connections in the available resources. A higher SB also means the same, but it also means that it suffers from spectrum fragmentation. Thus, it can be seen that in all the cases, TaTRA and TRA efficiently select the resources. The change in the balance point of trade-off for each MF is also justified based on the drastic change in the blocking types between different XT^{sp} values. We note that a higher QBE means the algorithm is not efficiently handling the trade-off and locking the free spectrum, which can be seen from the relationship between the blocking type in Fig. 6(a) and the BBP performance in Fig. 4(a). Similar observations can be made from Fig. 6(b) and the corresponding BBP performance in Fig. 4(f). Here, the iSC version of pTRA and TRA have

similar blocking; however, SB increases with TRA-rSC, meaning that it is able to manage the XT levels but the spectrum is now either not sufficient or fragmented. The effect of MC and SC on the blocking performance can be studied by comparing Figs. 6(a) and 6(b). Here, QBS and QBD dominate the other blocking types due to lower γ_d values because the path lengths are higher for TpNs compared to SMC-TlN for the restrictive TR model at $XT^{\text{sp}} = -40$ dB.

We have observed that the effect of each of the three contributors of TC has a different effect on the performance of TRA/TaTRA. Based on this observation, TRA/TaTRA with equal weights outperforms the baseline algorithms and algorithms in the literature for TpNs and both SMC and nSMC scenarios of translucent networks. We also explored the effect of various sets of weights on the performance of TRA/TaTRA under all the scenarios. The performance improves even further in some of the scenarios for particular sets of weights. We do not present those results in this paper and will consider a thorough investigation of various weights and their performance in a future study.

8. CONCLUDING REMARKS

We addressed the dynamic RMCSA problem in spectrally spatially flexible optical networks. Intercore crosstalk is an important consideration in MCF SS-FONs, and we proposed TRA, an RMCSA algorithm, and TaTRA, which achieve a good balance between spectrum utilization and crosstalk levels in TpNs and translucent networks. The algorithms consider network occupancy to calculate the capacity loss and select the spectrum that has the least effect on the network for future connections. The trade-off between spectrum utilization and crosstalk tolerance is properly handled using the effect of crosstalk in the calculation of capacity loss, which in turn results in a vastly better blocking performance of TRA and TaTRA over algorithms in the current literature.

Funding. National Science Foundation (CNS-1813617, CNS-1813772).

REFERENCES

1. O. Gerstel, M. Jinno, A. Lord, and S. B. Yoo, "Elastic optical networking: a new dawn for the optical layer?" IEEE Commun. Mag. **50**(2), s12–s20 (2012).
2. M. Klinkowski, P. Lechowicz, and K. Walkowiak, "Survey of resource allocation schemes and algorithms in spectrally-spatially flexible optical networking," Opt. Switching Netw. **27**, 58–78 (2018).
3. T. Hayashi, T. Taru, O. Shimakawa, T. Sasaki, and E. Sasaoka, "Design and fabrication of ultra-low crosstalk and low-loss multi-core fiber," Opt. Express **19**, 16576–16592 (2011).
4. W. Kmiecik and K. Walkowiak, "A performance study of dynamic routing algorithm for SDM translucent optical networks with assistive storage," Opt. Switching Netw. **38**, 100572 (2020).
5. H. M. Oliveira and N. L. da Fonseca, "Multipath routing, spectrum and core allocation in protected SDM elastic optical networks," in *IEEE Global Communications Conference (GLOBECOM)* (IEEE, 2019).
6. S. Petale, J. Zhao, and S. Subramaniam, "Tridental resource assignment algorithm for spectrally-spatially flexible optical networks," in *IEEE International Conference on Communications (ICC)* (IEEE, 2021).
7. Í. Brasileiro, L. Costa, and A. Drummond, "A survey on challenges of spatial division multiplexing enabled elastic optical networks," Opt. Switching Netw. **38**, 100584 (2020).
8. H. Tode and Y. Hirota, "Routing, spectrum and core assignment for space division multiplexing elastic optical networks," in *16th International Telecommunications Network Strategy and Planning Symposium (Networks)* (IEEE, 2014).
9. H. Tode and Y. Hirota, "Routing, spectrum and core assignment on SDM optical networks," in *Optical Fiber Communication Conference*, OSA Technical Digest (online) (Optica Publishing Group, 2016), paper Tu2H.1.
10. H. Tode and Y. Hirota, "Routing, spectrum, and core and/or mode assignment on space-division multiplexing optical networks," J. Opt. Commun. Netw. **9**, A99–A113 (2017).
11. S. Fujii, Y. Hirota, H. Tode, and K. Murakami, "On-demand spectrum and core allocation for reducing crosstalk in multicore fibers in elastic optical networks," J. Opt. Commun. Netw. **6**, 1059–1071 (2014).
12. Y. Zhao, Y. Zhu, C. Wang, X. Yu, C. Liu, B. Li, and J. Zhang, "Super-channel oriented routing, spectrum and core assignment under crosstalk limit in spatial division multiplexing elastic optical networks," Opt. Fiber Technol. **36**, 249–254 (2017).
13. M. Klinkowski and G. Zalewski, "Dynamic crosstalk-aware lightpath provisioning in spectrally-spatially flexible optical networks," J. Opt. Commun. Netw. **11**, 213–225 (2019).
14. Y. Tan, H. Yang, R. Zhu, Y. Zhao, J. Zhang, Z. Liu, Q. Ou, and Z. Zhou, "Distance adaptive routing, core and spectrum allocation in space division multiplexing optical networks with multi-core fibers," in *Asia Communications and Photonics Conference*, OSA Technical Digest (online) (Optica Publishing Group, 2016), paper AF2A.159.
15. M. Yang, Y. Zhang, and Q. Wu, "Routing, spectrum, and core assignment in SDM-EONS with MCF: node-arc ILP/MILP methods and an efficient XT-aware heuristic algorithm," J. Opt. Commun. Netw. **10**, 195–208 (2018).
16. Q. Yao, H. Yang, H. Xiao, Y. Zhao, R. Zhu, and J. Zhang, "Crosstalk-aware routing, spectrum, and core assignment in space-division multiplexing optical networks with multicore fibers," Opt. Eng. **56**, 066104 (2017).
17. B. C. Chatterjee, A. Wadud, I. Ahmed, and E. Oki, "Priority-based inter-core and inter-mode crosstalk-avoided resource allocation for spectrally-spatially elastic optical networks," IEEE/ACM Trans. Netw. **29**, 1634–1647 (2021).
18. M. Yang, K. Guo, Y. Zhang, and Y. Ji, "Routing, modulation level, spectrum and transceiver assignment in elastic optical networks," IEICE Trans. Commun. **E101.B**, 1197–1209 (2018).
19. M. Klinkowski and K. Walkowiak, "Performance analysis of flexible regeneration and modulation conversion in elastic optical networks," in *Optical Fiber Communication Conference*, OSA Technical Digest (online) (Optica Publishing Group, 2017), paper Th2A.13.
20. M. Klinkowski and K. Walkowiak, "On performance gains of flexible regeneration and modulation conversion in translucent elastic optical networks with superchannel transmission," J. Lightwave Technol. **34**, 5485–5495 (2016).
21. K. Walkowiak, M. Klinkowski, and P. Lechowicz, "Dynamic routing in spectrally spatially flexible optical networks with back-to-back regeneration," J. Opt. Commun. Netw. **10**, 523–534 (2018).
22. K. Walkowiak, A. Wlodarczyk, and M. Klinkowski, "Effective worst-case crosstalk estimation for dynamic translucent SDM elastic optical networks," in *IEEE International Conference on Communications (ICC)* (IEEE, 2019).
23. K. Walkowiak, P. Lechowicz, and M. Klinkowski, "Impact of inter-core crosstalk on performance of spectrally-spatially flexible optical networks with B2B regeneration," in *20th International Conference on Transparent Optical Networks (ICTON)* (IEEE, 2018).
24. K. Walkowiak, R. Goścień, P. Lechowicz, A. Włodarczyk, and M. Klinkowski, "Transponder placement for dynamic lightpath provisioning in survivable translucent optical networks," in *22nd International Conference on Transparent Optical Networks (ICTON)* (IEEE, 2020).
25. K. Walkowiak, M. Klinkowski, A. Włodarczyk, and A. Kasprzak, "Predeployment of transponders for dynamic lightpath provisioning in translucent spectrally–spatially flexible optical networks," Appl. Sci. **10**, 2802 (2020).
26. F. Arpanaei, N. Ardalani, H. Beyranvand, and S. A. Alavian, "Three-dimensional resource allocation in space division multiplexing elastic optical networks," J. Opt. Commun. Netw. **10**, 959–974 (2018).

27. F. Arpanaei, N. Ardalani, H. Beyranvand, and B. Shariati, "QoT-aware performance evaluation of spectrally–spatially flexible optical networks over FM-MCFs," J. Opt. Commun. Netw. **12**, 288–300 (2020).
28. M. Jafari-Beyrami, A. G. Rahbar, and S. Hosseini, "On-demand fragmentation-aware spectrum allocation in space division multiplexed elastic optical networks with minimized crosstalk and multipath routing," Comput. Netw. **181**, 107531 (2020).
29. A. Muhammad, G. Zervas, and R. Forchheimer, "Resource allocation for space-division multiplexing: optical white box versus optical black box networking," J. Lightwave Technol. **33**, 4928–4941 (2015).
30. A. Agrawal, V. Bhatia, and S. Prakash, "Core arrangement based spectrum-efficient path selection in core-continuity constrained SS-FONs," in *International IFIP Conference on Optical Network Design and Modeling* (Springer, 2019), pp. 570–583.
31. J. Zhu and Z. Zhu, "Physical-layer security in MCF-based SDM-EONs: would crosstalk-aware service provisioning be good enough?" J. Lightwave Technol. **35**, 4826–4837 (2017).
32. K. Saitoh and S. Matsuo, "Multicore fiber technology," J. Lightwave Technol. **34**, 55–66 (2016).
33. C. Rottondi, P. Martelli, P. Boffi, L. Barletta, and M. Tornatore, "Crosstalk-aware core and spectrum assignment in a multicore optical link with flexible grid," IEEE Trans. Commun. **67**, 2144–2156 (2018).
34. D. M. Marom and M. Blau, "Switching solutions for WDM-SDM optical networks," IEEE Commun. Mag. **53**(2), 60–68 (2015).
35. P. Poggiolini, "The GN model of non-linear propagation in uncompensated coherent optical systems," J. Lightwave Technol. **30**, 3857–3879 (2012).
36. B. Puttnam, R. Luis, T. Eriksson, W. Klaus, J.-M. D. Mendinueta, Y. Awaji, and N. Wada, "Impact of intercore crosstalk on the transmission distance of QAM formats in multicore fibers," IEEE Photon. J. **8**, 0601109 (2016).
37. J. Wu, S. Subramaniam, and H. Hasegawa, "Efficient dynamic routing and spectrum assignment for multifiber elastic optical networks," J. Opt. Commun. Netw. **11**, 190–201 (2019).
38. R. Goścień and M. Kucharzak, "On the efficient optimization of unicast, anycast and multicast flows in survivable elastic optical networks," Opt. Switching Netw. **31**, 114–126 (2019).